Biomedical Optics EXPRESS

Functional second harmonic generation microscopy probes molecular dynamics with high temporal resolution

Moritz Förderer,[1,2] Tihomir Georgiev,[1] Matias Mosqueira,[1] Rainer H. A. Fink,[1] and Martin Vogel[1,3,4]

[1]*Medical Biophysics Unit, Institute for Physiology and Pathophysiology, University of Heidelberg, Heidelberg, Germany*
[2]*m.foerderer@physiologie.uni-heidelberg.de*
[3]*Current address: Max Planck Institute of Biophysics, Frankfurt/Main, Germany*
[4]*martin.vogel@biophys.mpg.de*

Abstract: Second harmonic generation (SHG) microscopy is a powerful tool for label free *ex vivo* or *in vivo* imaging, widely used to investigate structure and organization of endogenous SHG emitting proteins such as myosin or collagen. Polarization resolved SHG microscopy renders supplementary information and is used to probe different molecular states. This development towards functional SHG microscopy is calling for new methods for high speed functional imaging of dynamic processes. In this work we present two approaches with linear polarized light and demonstrate high speed line scan measurements of the molecular dynamics of the motor protein myosin with a time resolution of 1 ms in mammalian muscle cells. Such a high speed functional SHG microscopy has high potential to deliver new insights into structural and temporal molecular dynamics under *ex vivo* or *in vivo* conditions.

OCIS codes: (180.4315) Nonlinear microscopy; (190.2620) Harmonic generation and mixing; (170.2655) Functional monitoring and imaging.

References and links

1. Y. Guo, P. P. Ho, H. Savage, D. Harris, P. Sacks, S. Schantz, F. Liu, N. Zhadin, and R. R. Alfano, "Second-harmonic tomography of tissues," Opt. Lett. **22**(17), 1323–1325 (1997).
2. P. J. Campagnola, A. C. Millard, M. Terasaki, P. E. Hoppe, C. J. Malone, and W. A. Mohler, "Three-dimensional high-resolution second-harmonic generation imaging of endogenous structural proteins in biological tissues," Biophys. J. **82**(1), 493–508 (2002).
3. M. Both, M. Vogel, R. H. Fink, and D. Uttenweiler, "Second harmonic generation imaging in muscle fibers," Proc. SPIE **5139**, 112–120 (2003).
4. M. Both, M. Vogel, O. Friedrich, F. von Wegner, T. Künsting, R. H. Fink, and D. Uttenweiler, "Second harmonic imaging of intrinsic signals in muscle fibers in situ," J. Biomed. Opt. **9**(5), 882–892 (2004).
5. S. V. Plotnikov, A. C. Millard, P. J. Campagnola, and W. A. Mohler, "Characterization of the myosin-based source for second-harmonic generation from muscle sarcomeres," Biophys. J. **90**(2), 693–703 (2006).
6. S. Schürmann, F. von Wegner, R. H. Fink, O. Friedrich, and M. Vogel, "Second harmonic generation microscopy probes different states of motor protein interaction in myofibrils," Biophys. J. **99**(6), 1842–1851 (2010).
7. S. Roth and I. Freund, "Second harmonic generation in collagen," J. Chem. Phys. **70**(4), 1637–1643 (1979).
8. M. E. Llewellyn, R. P. Barretto, S. L. Delp, and M. J. Schnitzer, "Minimally invasive high-speed imaging of sarcomere contractile dynamics in mice and humans," Nature **454**(7205), 784–788 (2008).
9. S. V. Plotnikov, A. M. Kenny, S. J. Walsh, B. Zubrowski, C. Joseph, V. L. Scranton, G. A. Kuchel, D. Dauser, M. Xu, C. C. Pilbeam, D. J. Adams, R. P. Dougherty, P. J. Campagnola, and W. A. Mohler, "Measurement of muscle disease by quantitative second-harmonic generation imaging," J. Biomed. Opt. **13**(4), 044018 (2008).
10. A. Buttgereit, C. Weber, C. S. Garbe, and O. Friedrich, "From chaos to split-ups--SHG microscopy reveals a specific remodelling mechanism in ageing dystrophic muscle," J. Pathol. **229**(3), 477–485 (2013).
11. W. Liu, N. Raben, and E. Ralston, "Quantitative evaluation of skeletal muscle defects in second harmonic generation images," J. Biomed. Opt. **18**(2), 026005 (2013).
12. G. Recher, P. Coumailleau, D. Rouède, and F. Tiaho, "Structural origin of the drastic modification of second harmonic generation intensity pattern occurring in tail muscles of climax stages xenopus tadpoles," J. Struct. Biol. **190**(1), 1–10 (2015).

#254217 Received 18 Nov 2015; revised 18 Dec 2015; accepted 18 Dec 2015; published 15 Jan 2016

13. E. Ralston, B. Swaim, M. Czapiga, W. L. Hwu, Y. H. Chien, M. G. Pittis, B. Bembi, O. Schwartz, P. Plotz, and N. Raben, "Detection and imaging of non-contractile inclusions and sarcomeric anomalies in skeletal muscle by second harmonic generation combined with two-photon excited fluorescence," J. Struct. Biol. **162**(3), 500–508 (2008).
14. F. Légaré, C. Pfeffer, and B. R. Olsen, "The role of backscattering in SHG tissue imaging," Biophys. J. **93**(4), 1312–1320 (2007).
15. A. Wingert, H. Seim, S. Schürmann, R. H. A. Fink, and M. Vogel, "Signal Efficiency in Gradient Index Lens Based Two Photon Microscopy," Open J. Biophys. **3**(1), 43–50 (2013).
16. T. Boulesteix, E. Beaurepaire, M. P. Sauviat, and M. C. Schanne-Klein, "Second-harmonic microscopy of unstained living cardiac myocytes: measurements of sarcomere length with 20-nm accuracy," Opt. Lett. **29**(17), 2031–2033 (2004).
17. S. J. Wallace, J. L. Morrison, K. J. Botting, and T. W. Kee, "Second-harmonic generation and two-photon-excited autofluorescence microscopy of cardiomyocytes: quantification of cell volume and myosin filaments," J. Biomed. Opt. **13**(6), 064018 (2008).
18. S. Psilodimitrakopoulos, D. Artigas, G. Soria, I. Amat-Roldan, A. M. Planas, and P. Loza-Alvarez, "Quantitative discrimination between endogenous SHG sources in mammalian tissue, based on their polarization response," Opt. Express **17**(12), 10168–10176 (2009).
19. C. Odin, T. Guilbert, A. Alkilani, O. P. Boryskina, V. Fleury, and Y. Le Grand, "Collagen and myosin characterization by orientation field second harmonic microscopy," Opt. Express **16**(20), 16151–16165 (2008).
20. S. Psilodimitrakopoulos, S. I. Santos, I. Amat-Roldan, A. K. Thayil, D. Artigas, and P. Loza-Alvarez, "In vivo, pixel-resolution mapping of thick filaments' orientation in nonfibrilar muscle using polarization-sensitive second harmonic generation microscopy," J. Biomed. Opt. **14**(1), 014001 (2009).
21. G. Recher, D. Rouède, P. Richard, A. Simon, J. J. Bellanger, and F. Tiaho, "Three distinct sarcomeric patterns of skeletal muscle revealed by SHG and TPEF microscopy," Opt. Express **17**(22), 19763–19777 (2009).
22. D. G. Winters, D. R. Smith, P. Schlup, and R. A. Bartels, "Measurement of orientation and susceptibility ratios using a polarization-resolved second-harmonic generation holographic microscope," Biomed. Opt. Express **3**(9), 2004–2011 (2012).
23. S. Brasselet, "Polarization-resolved nonlinear microscopy: application to structural molecular and biological imaging," Adv. Opt. Photonics **3**(3), 205–271 (2011).
24. N. Mazumder, C. W. Hu, J. Qiu, M. R. Foreman, C. M. Romero, P. Török, and F. J. Kao, "Revealing molecular structure and orientation with Stokes vector resolved second harmonic generation microscopy," Methods **66**(2), 237–245 (2014).
25. V. Nucciotti, C. Stringari, L. Sacconi, F. Vanzi, L. Fusi, M. Linari, G. Piazzesi, V. Lombardi, and F. S. Pavone, "Probing myosin structural conformation in vivo by second-harmonic generation microscopy," Proc. Natl. Acad. Sci. U.S.A. **107**(17), 7763–7768 (2010).
26. J. R. Blinks, R. Rüdel, and S. R. Taylor, "Calcium transients in isolated amphibian skeletal muscle fibres: detection with aequorin," J. Physiol. **277**(1), 291–323 (1978).
27. C. H. Lien, K. Tilbury, S. J. Chen, and P. J. Campagnola, "Precise, motion-free polarization control in Second Harmonic Generation microscopy using a liquid crystal modulator in the infinity space," Biomed. Opt. Express **4**(10), 1991–2002 (2013).
28. S. Psilodimitrakopoulos, P. Loza-Alvarez, and D. Artigas, "Fast monitoring of in-vivo conformational changes in myosin using single scan polarization-SHG microscopy," Biomed. Opt. Express **5**(12), 4362–4373 (2014).
29. D. A. Kleinman, "Nonlinear dielectric polarization in optical media," Phys. Rev. **126**(6), 1977–1979 (1962).
30. F. Tiaho, G. Recher, and D. Rouède, "Estimation of helical angles of myosin and collagen by second harmonic generation imaging microscopy," Opt. Express **15**(19), 12286–12295 (2007).
31. C. Teulon, I. Gusachenko, G. Latour, and M. C. Schanne-Klein, "Theoretical, numerical and experimental study of geometrical parameters that affect anisotropy measurements in polarization-resolved SHG microscopy," Opt. Express **23**(7), 9313–9328 (2015).
32. I. Gusachenko, G. Latour, and M. C. Schanne-Klein, "Polarization-resolved Second Harmonic microscopy in anisotropic thick tissues," Opt. Express **18**(18), 19339–19352 (2010).
33. S. Brasselet, D. Aït-Belkacem, A. Gasecka, F. Munhoz, S. Brustlein, and S. Brasselet, "Influence of birefringence on polarization resolved nonlinear microscopy and collagen SHG structural imaging," Opt. Express **18**(14), 14859–14870 (2010).
34. O. Friedrich, T. Ehmer, and R. H. A. Fink, "Calcium currents during contraction and shortening in enzymatically isolated murine skeletal muscle fibres," J. Physiol. **517**(3), 757–770 (1999).
35. A. Leray, L. Leroy, Y. Le Grand, C. Odin, A. Renault, V. Vié, D. Rouède, T. Mallegol, O. Mongin, M. H. V. Werts, and M. Blanchard-Desce, "Organization and orientation of amphiphilic push-pull chromophores deposited in Langmuir-Blodgett monolayers studied by second harmonic generation and atomic force microscopy," Langmuir **20**(19), 8165–8171 (2004).
36. D. Rouède, J. J. Bellanger, J. Bomo, G. Baffet, and F. Tiaho, "Linear least square (LLS) method for pixel-resolution analysis of polarization dependent SHG images of collagen fibrils," Opt. Express **23**(10), 13309–13319 (2015).
37. C. K. Chou, W. L. Chen, P. T. Fwu, S. J. Lin, H. S. Lee, and C. Y. Dong, "Polarization ellipticity compensation in polarization second-harmonic generation microscopy without specimen rotation," J. Biomed. Opt. **13**(1), 014005 (2008).

#254217 Received 18 Nov 2015; revised 18 Dec 2015; accepted 18 Dec 2015; published 15 Jan 2016

38. A. E. Tuer, M. K. Akens, S. Krouglov, D. Sandkuijl, B. C. Wilson, C. M. Whyne, and V. Barzda, "Hierarchical model of fibrillar collagen organization for interpreting the second-order susceptibility tensors in biological tissue," Biophys. J. **103**(10), 2093–2105 (2012).

1. Introduction

Since the discovery of second harmonic generation (SHG) signals generated in endogenous proteins like myosin in muscle [1–6] or collagen [2, 7] various advances in this field of microscopy have been established: The intrinsic nature of the SHG signal allows for label free and high contrast imaging under *in vivo* [8] or *ex vivo* [2] conditions, thus making SHG microscopy a powerful tool in biomedical research. With muscle samples, structural SHG (sSHG) microscopy is used to investigate structural changes down to the sarcomeric level for a wide range of biomedical questions and applications [9–13]. Back scattered SHG signal [14, 15] is of high interest for diagnostic applications and led to minimally invasive approaches [8]. Research on cardiomyocytes demonstrates its potential use for heart correlated myopathies [16, 17].

The coherent SHG process reveals a characteristic polarization dependency that, for certain sample symmetries and assumptions, can be described by a single parameter which we denoted γ in an earlier study [4]. γ can be used for polarization sensitive measurements [18]. Subsequently, polarization resolved sSHG microscopy was performed by measuring over a range of polarization angles of the incident laser beam, at different characteristic angles, by splitting the SHG signal itself in different polarizations or by using Stokes vector analysis [19–24] to gather information of structural order and orientation. By demonstrating the changes in the polarization dependent SHG signal due to conformational changes of the motor protein myosin in different contraction states of muscle (rigor or relaxed state, isometric tetanic contraction) [6, 25] first steps towards a *functional* SHG (fSHG) have been realized. These results aim for a method that allows retrieving functional information on the molecular level during muscle contraction.

Yet, the time needed for measurements over a wide range of polarization angles (approximately 1s in reference [25]) is not suitable for high speed measurements with millisecond time resolution, mandatory to resolve the molecular dynamics of the contraction process with its typical time range of a few tens to a few hundreds of milliseconds [26]. Even the use of e.g. a liquid crystal modulator for polarization control is not fast enough for this purpose [27]. Recently, a first promising approach using circular polarized light was proposed by Psilodimitrakopoulos *et al*. [28]. Using three PMT detectors for collection of three different polarization states of the SHG signal and with the use of incident light with circular polarization they performed two-dimensional single scan measurements with a time resolution of one frame per second under *in vivo* conditions. As such, they monitored cooperation of different muscle regions and elegantly underwent the polarization angle dependency of the SHG signal as they calculated the angle of the sample with respect to the detection system. But the production of high quality circular polarization in the incident laser beam and the integration of three PMTs into the detection system of a standard laser scanning microscope can be experimentally challenging. With respect to data analysis, residual ellipticity in the laser beam may cause systematic errors as the calculation of the sample angle is based on the assumption of perfect circular polarization.

To overcome these potential difficulties, we developed two approaches that both employ linear polarized incident light at a fixed single angle and that make use of one or two PMT detectors only for *ex vivo* applications. Furthermore, we demonstrate high speed line scan measurements with millisecond time resolution during muscle contraction, constituting another important step to establish fast functional SHG microscopy in order to investigate molecular dynamics.

#254217 Received 18 Nov 2015; revised 18 Dec 2015; accepted 18 Dec 2015; published 15 Jan 2016

2. Materials and methods

2.1 Theoretical considerations

The second order polarization of a nonlinear medium induced by an incident electrical field of a light wave is given by [4]:

$$P_i = \sum_{jk} \chi_{ijk} E_j E_k, \tag{1}$$

where χ(ijk) are components of the second order susceptibility tensor. Assuming cylindrical symmetry of a muscle fiber positioned along the x-axis, Kleinman symmetry [29] and a laser beam with the axis of linear polarization in the x-y-plane, the intensities of the x and y polarization components of the emitted SHG signal are given by [23]:

$$\begin{aligned} I_x(\alpha) &= B\chi_{xyy}^2 \left[\gamma \cos^2(\alpha) + \sin^2(\alpha)\right]^2, \\ I_y(\alpha) &= B\chi_{xyy}^2 \left[\sin(2\alpha)\right]^2, \end{aligned} \tag{2}$$

with

$$\gamma = \frac{\chi_{xxx}}{\chi_{xyy}}. \tag{3}$$

The total SHG intensity is I(α) = Ix(α) + Iy(α). α is the angle of the polarization with respect to the x-axis (and therefore the sample) and B is a proportionality factor given by the local experimental conditions (note that the χ^2(xyy) factor is commonly included in B). In this model, the two tensor components χ(xxx), χ(xyy) and the parameter γ are the only remaining structural parameters. They completely describe the nonlinear response of the sample. Hence, they probe molecular conformational changes with a change of their values [6, 25] and give information about the mean orientation of SHG emitters [30]. The experimentally observed angular dependencies of the polarization components Ix and Iy were compatible with the model laid out in Eq. (2).

Method #1

A ratiometric approach of measuring the change between two different states S1 and S2 of the sample (e.g., rigor and relaxed state of muscle) involves the recording of the SHG signal at polarization angles of 0° or 90°, respectively. This renders information about the relative change of the two tensor components mentioned in Eq. (3):

$$\begin{aligned} \frac{\chi_{xxx}^{(S2)}}{\chi_{xxx}^{(S1)}} &= \sqrt{\frac{I^{(S2)}(0°)}{I^{(S1)}(0°)}}, \\ \frac{\chi_{xyy}^{(S2)}}{\chi_{xyy}^{(S1)}} &= \sqrt{\frac{I^{(S2)}(90°)}{I^{(S1)}(90°)}}. \end{aligned} \tag{4}$$

Thus, recording at one specific angle of polarization only, this method allows monitoring the two tensor components separately. Note that there is no need to split the SHG signal onto multiple detectors. As a control for comparison to existing data we can use the ratio of the ratios defined in Eq. (4), which describes the relative change of γ itself:

$$\frac{\gamma^{(S2)}}{\gamma^{(S1)}} = \left(\frac{\chi_{xxx}^{(S2)}}{\chi_{xxx}^{(S1)}}\right) \Big/ \left(\frac{\chi_{xyy}^{(S2)}}{\chi_{xyy}^{(S1)}}\right). \tag{5}$$

#254217 Received 18 Nov 2015; revised 18 Dec 2015; accepted 18 Dec 2015; published 15 Jan 2016

Method #2

For the second method, the SHG signal is split into its x- and y- polarization components Ix and Iy that are detected on two detectors simultaneously. Then, γ can be determined using a polarimetric approach, where the measurement is taken at one angle of polarization α only:

$$\gamma = \tan(\alpha)\left[2\sqrt{\frac{I_x(\alpha)}{I_y(\alpha)}} - \tan(\alpha)\right]. \tag{6}$$

This equation is defined for 0°< α <90° only. For angles of 90°< α <180° the sign before the root changes as we assume that γ is always positive.

A single angle approach enables high speed line scans and therefore recordings of the signal change during, e.g., contraction. To minimize artifacts caused by sample movements we determined a range of polarization angles where systematic errors and movement of the sample have minimum impact on the difference between the 'real' γ and its measured counterpart γ*:

$$\gamma^* = \tan(\alpha)\left[2\sqrt{\frac{I_x^*}{I_y^*}} - \tan(\alpha)\right], \tag{7}$$

with

$$\frac{I_x^*}{I_y^*} = \frac{I_x \cos^2(\Delta\beta - \Delta\varphi) + I_y \sin^2(\Delta\beta - \Delta\varphi) + \sin\left(2(\Delta\beta - \Delta\varphi)\right)\sqrt{I_x I_y}}{I_x \sin^2(\Delta\beta - \Delta\varphi) + I_y \cos^2(\Delta\beta - \Delta\varphi) - \sin\left(2(\Delta\beta - \Delta\varphi)\right)\sqrt{I_x I_y}},$$

and

$$I_x = I_x(\alpha + \Delta\alpha - \Delta\varphi),$$
$$I_y = I_y(\alpha + \Delta\alpha - \Delta\varphi).$$

Δα is the systematic inaccuracy of the polarization angle setting, Δβ the systematic inaccuracy of the polarizing beam splitter setting, Δφ represents the misalignment of the sample with respect to the x-axis, α is the assumed polarization angle and $I_{x,y}^*$ (later on denoted as ()*) are the actual measured signals. Note that same or opposite signs of Δα and Δβ lead to different angle ranges of minimized impact. We identified an ideal situation where we have same signs and comparable size of Δα and Δβ. This situation is mathematically equivalent to a misalignment of the sample and leads to an optimal range of angles around 20°. In general, a major discrepancy of Δα and Δβ is disadvantageous. For reasonable systematic inaccuracies, a major discrepancy is primarily created by opposite signs. Based on the model of Eq. (7), we chose α = 18° for our measurements. To determine this optimized value for α we used the (uncorrected) γ values reported in [6]. In general, common approximations like neglecting an axial component of the polarization at high NA [6, 31] or birefringence [32, 33] were used for this first proof of principle.

2.2 Setup

The microscope setup used for this study has been described previously [4, 6]. In short, the setup is based on a confocal laser scanning setup (TCS SP2 MP, Leica Microsystems, Mannheim, Germany) and an inverted microscope (DM IRBE, Leica) for fluorescence imaging. For SHG microscopy, a mode-locked ps-pulsed Ti:Sa laser (Tsunami, Spectra Physics, Irvine, CA) with a pulse duration of approximately 2 ps and a repetition rate of approximately 80 MHz is coupled into the system with the fundamental laser wavelength tuned to ~880 nm. A half-wave plate (HWP) (B. Halle, Berlin, Germany) fixed to a custom-

#254217 Received 18 Nov 2015; revised 18 Dec 2015; accepted 18 Dec 2015; published 15 Jan 2016

build rotation stage with an angle scale is installed below the objective's back aperture to manipulate the polarization angle of the laser beam (Fig. 1(A)). The quality of the linear polarization was better than 1:60 after the HWP. The laser beam is focused by a 63x NA 1.2 water immersion objective (PL APO 63x NA 1.20 W Corr, Leica) into the object plane. The transmitted signal is collected by an identical objective mounted in a nose-to-nose configuration. The signal can be split with a polarizing beam splitter (PBS) (G335564000, Linos, Göttingen, Germany) and detected with two photomultiplier tubes (PMT) (R6357 and R9624, Hamamatsu, Hamamatsu City, Japan) of the setup. In addition to IR filters, band pass filters (BP) can be brought into the optical pathway.

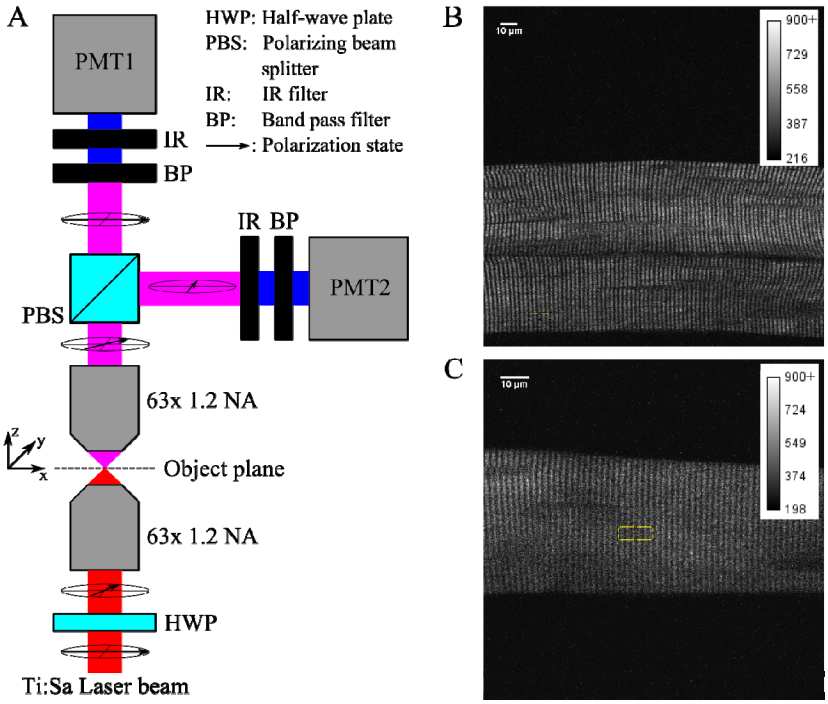

Fig. 1. (**A**) Setup configuration prepared to detect the Ix and Iy components of the SHG signal. (**B**) Sample image of the Ix SHG signal generated in a skinned EDL fiber bundle in relaxed state with a sample ROI (marked in yellow). (**C**) Sample image of the Iy SHG signal generated in a resting intact IO fiber with a sample ROI. For visualization purposes, pixels with very large gray values are displayed in white (occurrence <0.01% of total number of pixels).

Measurements of method #1 were recorded with PMT #1 without the PBS. For non-dynamic measurements of method #2, only PMT #1 was used and the polarization signals were recorded consecutively by turning the PBS by 90°. For dynamic measurements both PMTs were used. Calibration was performed by measuring the signal of a sample with PMT #2 at different laser powers and then with PMT #1 after turning the PBS by 90°. This way both PMTs recorded the same signal and the results were fitted with a square function – total SHG signal is proportional to the square of the laser power – allowing us to cross-calibrate the signals emerging from both PMTs. The angular positions of the HWP and the PBS with respect to their scales could be set with an accuracy of better than 0.5°. The scales were calibrated with respect to the scan direction of the microscope which was defined as the x-axis in the lab coordinate system.

The sample holders were set into a rotation stage so that they could be aligned in parallel to the scan direction such that the myosin bands were perpendicular to the scan direction. All images were recorded and digitized with 12-bit resolution. Image analysis was performed

#254217 Received 18 Nov 2015; revised 18 Dec 2015; accepted 18 Dec 2015; published 15 Jan 2016

with ImageJ software (Rasband, W.S., ImageJ, U. S. National Institutes of Health, Bethesda, Maryland, USA, http://imagej.nih.gov/ij/, 1997-2015). To subtract the signal background, it was measured in a separate region of interest (ROI) in the same image for 2D images. For 1D line scans, it was measured in a separate line scan next to the sample. The average laser power at the back aperture of the objective before the HWP was set to approximately 150-190 mW.

2.3 Sample preparation

C57BL/6 wild type (wt) mice were sacrificed according to the guidelines of the state of Baden-Wuerttemberg and have been approved by the Regierungspräsidium Karlsruhe (permit number 83/14). For the measurements, skeletal muscle fiber bundles of dissected *Extensor Digitorum Longus* (EDL) and cells of enzymatically digested *Interossei* (IO) were used.

Whole EDL muscles were dissected in mouse Ringer solution (145 mM NaCl, 5 mM KCl, 2.5 mM $CaCl_2$, 10 mM Hepes, 1 mM $MgCl_2$, pH set to 7.4 with NaOH) and brought into High Relax (HR) solution (30 mM Hepes, 6.25 mM $Mg(OH)_2$, 30 mM EGTA, 8 mM Na_2ATP, 10 mM Na_2CP, pH set to 7.0 with KOH). Then, bundles of few fibers were dissected and mounted on two parallel stripes of double sticky tape (Fotostrip, Tesa, Norderstedt, Germany) between two cover slips. Cells were permeabilized with saponin in HR solution for 5 minutes and then washed several times either with HR or Rigor solution (30 mM Hepes, 0.4 mM $Mg(OH)_2$, 30 mM EGTA, 18 mM HDTA, 18 mM Na_2CO_3, pH set to 7.0 with KOH). For measurements using method #1, cells were first put into rigor state and the solution was changed during the measurement. Due to movement of the sample during solution change and change of state the sample position had to be corrected over the measurements but subsequent ROIs were chosen as close as possible to the initial ones. For method #2, rigor and relaxed state were measured separately in different samples. In Fig. 1(B) an EDL fiber bundle in relaxed state is shown with an exemplary ROI.

Single intact IO cells were prepared via digestion with collagenase based on a slightly varied protocol from [34]: The IO muscles were digested with 2-2.5 mg collagenase (Sigma-Aldrich, St Louis, MO, USA) in 3 ml Ringer solution for 40-50 minutes at 30-32°C and subsequently washed several times with Ringer solution. After at least one hour of incubation, the cells were separated mechanically via pipetting. Cells were used at maximum 30 hours after digestion and were kept in ringer solution at approximately 12°C. Just before the measurements, cells were either placed in Ringer solution between two cover slips or, for electrical stimulation, were embedded in a drop of 5% low melt agarose (Carl Roth, Karlsruhe, Germany) with surrounding ringer solution between two cover slips. In Fig. 1(C) a resting intact IO fiber in Ringer solution and an exemplary ROI are shown. For electrical stimulation two custom build and chlorided silver electrodes were used. For 1D line scanning, a line of interest instead of a rectangle ROI is chosen for scanning. For calcium imaging the cells were stained with 12.5 µmol/l Fluo-4 AM (Molecular Probes, Eugene, Oregon, USA) for 10 minutes and excited with a laser line at 488 nm. The calcium signal was then collected with the fluorescence confocal detection system of the Leica system. Experiments were carried out at room temperature.

For measurements of the rigor and relaxed state on chemically skinned fibers we chose EDL fiber bundles because long samples could be easily dissected. Long samples were necessary to immobilize the cells while a change of solutions for chemical preparation of the contraction states was still possible. These chemically prepared EDL fibers were used for a first proof of concept on non-dynamic samples. For dynamic measurements and electrical stimulation intact cells, *i.e.* with intact cell membranes, were required. Such intact cells can be easily prepared with enzymatically digested IO muscles. In addition, smaller fibers were preferable for transfer into the flow cell without damaging the fibers and for immobilization with agarose. For measurements of the accuracy of method #2 we also chose intact resting IO fibers to measure under conditions close to the dynamic measurements.

#254217 Received 18 Nov 2015; revised 18 Dec 2015; accepted 18 Dec 2015; published 15 Jan 2016

3. Results

3.1 Non-dynamic measurements

Method #1

As first step we performed non-dynamic measurements to test the validity of the methods and to compare the results to existing data. To examine the relative change of the individual tensor components (method #1, see above) from relaxed state to rigor state - the two extreme states of contraction - we performed measurements with chemically skinned EDL fiber bundles (N = 8 fibers; n = 8 ROIs). The fiber bundles were prepared for rigor state and subsequently changed to relaxed state during the measurements. 2D images were recorded for 0° and 90° polarization in each state with these settings: scan speed (SSP): 400 Hz, format (F): 512x512, frame average (AV): 2, image dimension (D): 238.04 µm x 238.04 µm.

We obtained a ratio of 2.3 ± 0.4 (mean ± standard deviation) for the $\chi(xxx)$ and 1.5 ± 0.2 for the $\chi(xyy)$ tensor component (see panel A of Fig. 2). For the calculation the rigor state was defined as the S2 state. Both tensor components $\chi(xxx)$ and $\chi(xyy)$ underwent an increase during a change from relaxed to rigor state, where the increase of $\chi(xxx)$ was substantially higher than the one of $\chi(xyy)$. The parameter γ mentioned above can serve as a control that a change of state has indeed taken place. As γ can also be determined by SHG intensity measurements at two angles of polarization, I(0°) and I(90°) [25],

$$\gamma = \sqrt{\frac{I(0°)}{I(90°)}}, \tag{8}$$

these control values were calculated for each ROI with Eq. (8) and are displayed in panel B of Fig. 2.

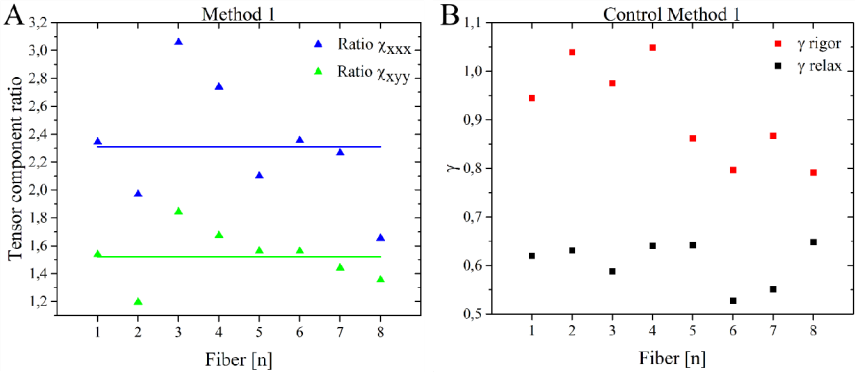

Fig. 2. Measurement results gathered with method #1. (**A**) Relative change of the tensor components $\chi(xxx)$ (blue) and $\chi(xyy)$ (green) following a conformational change in EDL fiber bundles from rigor to relaxed state. Mean values of the ratios were 2.3 ± 0.4 (mean ± standard deviation) for the $\chi(xxx)$ and 1.5 ± 0.2 for the $\chi(xyy)$ tensor component (see Eq. (4), the rigor state is defined as S2). (**B**) Control values of γ for relaxed (black dots) and rigor state (red dots) of the same ROIs calculated with Eq. (8).

Method #2

For method #2, we again started with non-dynamic measurements for validation. First, we determined if our chosen angle of polarization of 18° based on the model of Eq. (7) is a suitable choice: Varying the angle of polarization between 18°, 40° and 60°, we recorded measurements with resting IO fibers (N = 5; n = 5; SSP: 400 Hz, F: 512x512, AV: 2, ID: 119.05 µm x 119.05 µm). We compared the resulting mean γ values and their standard deviations to the control values gathered with Eq. (8) via measurements at 0° and 90° polarization (see Table 1). Additionally, we analyzed ROIs of inclined sarcomere structures

#254217 Received 18 Nov 2015; revised 18 Dec 2015; accepted 18 Dec 2015; published 15 Jan 2016

(n = 5) to examine the impact of misalignment of the samples at the different angles of polarization (inclination up to approximately 10°) (see Table 1). The angle of polarization of 18° matches best the control values in both cases.

Table 1. Comparison of control values to the γ values (mean ± standard deviation) of resting IO fibers measured with method #2 for different polarization angles. In addition to ROIs with myosin bands perpendicular to the scan direction (denoted as "exact ROI") ROIs with inclined bands were analyzed (denoted as "inclined ROI").

	Control	18° polarization	40° polarization	60° polarization
Exact ROI	0.61 ± 0.04	0.62 ± 0.05	0.63 ± 0.11	0.58 ± 0.36
Inclined ROI	0.62 ± 0.07	0.63 ± 0.11	0.70 ± 0.15	0.97 ± 0.60

Next, we performed non-dynamic measurements on small bundles of skinned EDL fibers in either relaxed (N = 8; n = 12) or rigor state (N = 10; n = 12) (SSP: 400 Hz, F: 512x512, AV: 3, ID: 198.39 µm x 198.39 µm). In Fig. 3(A) we show the results with γ values of 0.45 ± 0.08 (mean ± standard deviation) for the relaxed state and 0.70 ± 0.08 for the rigor state. Only fibers lying completely in the object plane (*i.e.*, no additional axial z-dependency) with visible striated pattern were taken into account. Figure 3(B) shows the results for the control, relaxed state 0.45 ± 0.04 and rigor state 0.75 ± 0.06. Our results were in good agreement with the control.

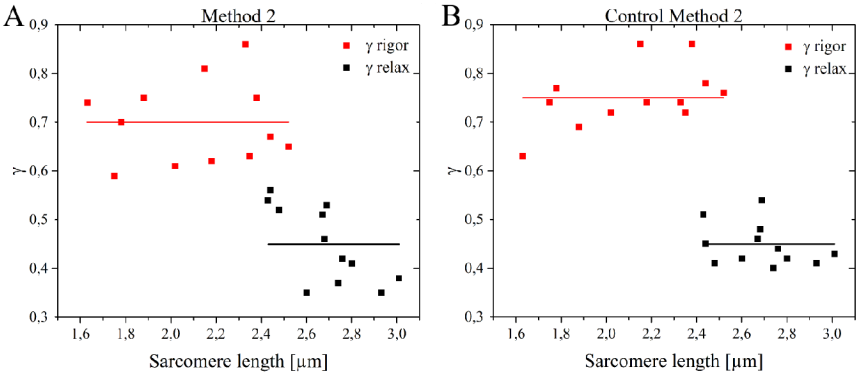

Fig. 3. Measurement results gathered with method #2 (single angle polarimetric approach) at a polarization angle of 18°. (**A**) Parameter γ on EDL fiber bundles in relaxed and rigor state. Results were 0.45 ± 0.08 (mean ± standard deviation) for relaxed state (black line) and 0.70 ± 0.08 for rigor state (red line), respectively. (**B**) Control values for γ: 0.45 ± 0.04 for relaxed state, 0.75 ± 0.06 for rigor state.

Then, we quantified the accuracy of method #2, *i.e.* the sensitivity to angular errors due to sideways movement of the sample during contraction that would lead to false changes of γ. Note that because of the intrinsic normalization a change of focus should not affect the results. As it was not possible to turn the sample precisely while keeping the same ROI, we simulated a sample misalignment by simultaneously turning the angle of polarization and the polarizing beam splitter in steps of 2° from + 10° to −10°. This way, we created effective angular errors of the sample from −10° to + 10°. Measurements were performed on resting IO fibers (N = 4; n = 8; SSP: 400 Hz, F: 512x512, AV: 2, ID: 119.05 µm x 119.05 µm). The mean γ values were calculated with Eq. (6) and with an assumed angle of polarization of 18° and they are shown in Fig. 4(A) for the different angular errors of the sample. The red dots represent γ* values of the model calculated with Eq. (7) where we assume that the systematic errors of the polarization calibration Δα and the PBS Δβ are −1.5° and −2°, respectively. Another assumption is that the γ value is the mean value of 0° of the experimental data. Note that these assumptions result already in a minor deviation of γ* at 0° while this change is already included in the experimental data. Ix and Iy were calculated with Eq. (2) by setting $B\chi^2(xyy) = 1$. Figure 4(B) depicts the relative deviation of γ compared to the value of no misalignment (0°). The individual signals of Ix and Iy are shown in Panel C (experimental

#254217 Received 18 Nov 2015; revised 18 Dec 2015; accepted 18 Dec 2015; published 15 Jan 2016

data). The values of the model, (Ix)* and (Iy)* (see Eq. (7)), corresponding to the model values of γ* in Panel A are shown in Panel D. The analysis of the individual signals is a powerful tool to identify false changes of γ due to movement of the sample (see section 4. Discussion).

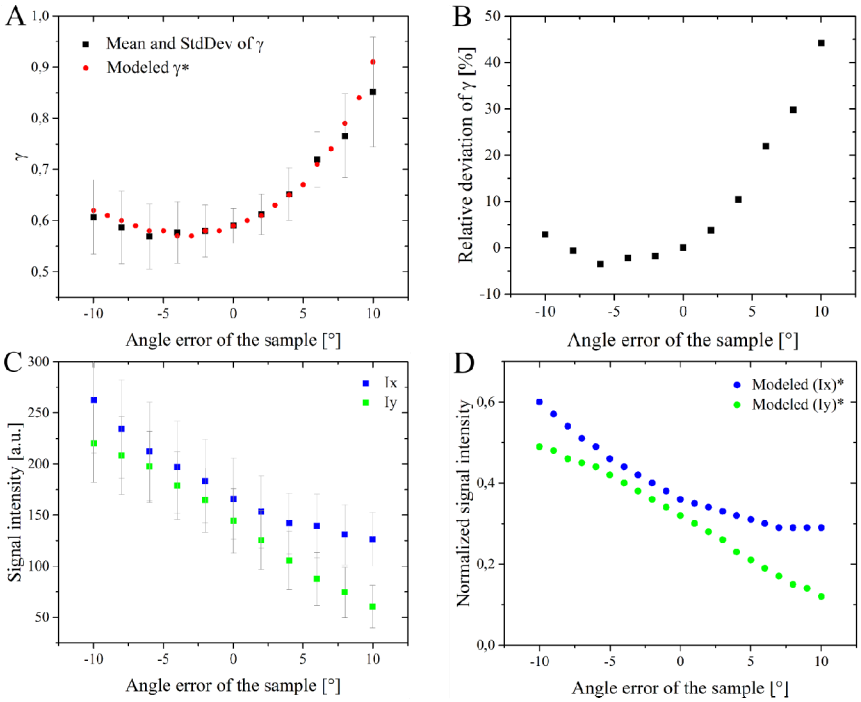

Fig. 4. Analysis of the impact of sideways shifts of the sample on the parameter γ in resting IO fibers with method #2 for angular errors of −10° to + 10°: the polarization angle and the PBS were simultaneously turned from + 10 to −10°. (**A**) Mean values and standard deviations of parameter γ at different angular errors of the sample (black) and the modeled values γ* (red) calculated with Eq. (7) assuming an inaccuracy of −1.5° for the polarization angle and −2° for the PBS and using the γ(0°) value of the experimental data. Ix and Iy were calculated with Eq. (2) by setting $B\chi^2(xyy) = 1$. (**B**) Relative deviation of γ from γ(0°). (**C**) Mean values and standard deviations of the Ix and Iy signal. (**D**) Normalized values of the model for (Ix)* and (Iy)* corresponding to the modeled values in panel A.

3.2 Dynamic measurements

After the feasibility of our polarimetric approach had been demonstrated in non-dynamic measurements, we tested method #2 for high speed 1D line scan measurements with millisecond time resolution on dynamic samples. Thus, we electrically stimulated intact IO fibers at a low level. The fibers were embedded in 5% low melting agarose to constrain the cells and prevent major movements. A line in the 2D image was chosen were myosin bands were perpendicular to the x-axis for line scanning with 1000 Hz. The Ix and Iy signals were recorded simultaneously.

#254217 Received 18 Nov 2015; revised 18 Dec 2015; accepted 18 Dec 2015; published 15 Jan 2016

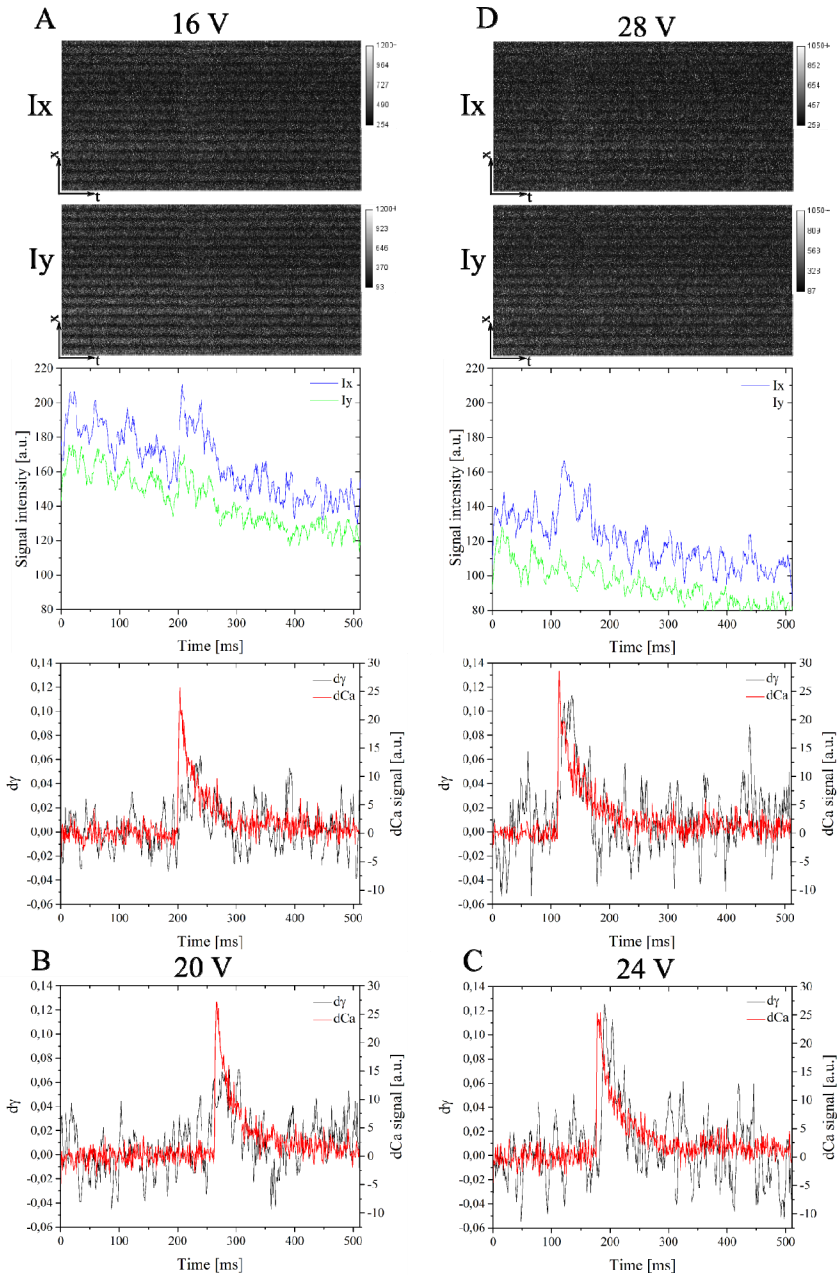

Fig. 5. Series of high speed line scans of an electrically stimulated IO fiber embedded in 5% low melting agarose at increasing voltages (see panels A, B, C, D) and 0.5 ms pulse duration: (**A**) 16V with the raw line scans for Ix and Iy (29.76µm x 512 ms), the differential γ signal (dγ, black) and differential calcium signal (dCa, red) and the Ix (blue) and Iy (green) signals. (**B**) Differential signals of γ and calcium for 20 V. (**C**) Differential signals of γ and calcium for 24 V. (**D**) Same as A for 28 V. dγ and Ix, Iy values were processed with a 5 point moving-window-average in all panels. For visualization purposes pixels with large gray values are displayed in white in the images (occurrence <0.1% of total number of pixels).

To monitor whether the cells were stimulated and whether contraction took place in the area of the chosen ROI, we simultaneously measured the calcium transient with the calcium indicator Fluo-4. Figure 5 shows the results of high speed measurements of the molecular

#254217 Received 18 Nov 2015; revised 18 Dec 2015; accepted 18 Dec 2015; published 15 Jan 2016

dynamics during contraction of an electrically stimulated IO fiber. A series of 4 different voltages from 16 V to 28 V in steps of 4V with 0.5 ms pulse duration was recorded (SSP: 1000 Hz, F: 256, ID: 29.76μm x 512 ms). The differential calcium signals and the differential γ signals are depicted in red and black, respectively. The signal before the peak was fitted with a line parallel to the x-axis to define the mean resting γ or calcium value which was then subtracted from all data points. Mean resting γ was between 0.59 and 0.61 for the four voltages. Note that these values for resting IO fibers and the values for the exact ROI in Table 1 were in between the values we obtain for the relaxed and for the rigor state with method #2. In Fig. 5(A) and 5(D) the corresponding line scan images and the Ix and Iy polarization signals are shown additionally in blue and green, respectively. The dγ signals and the Ix and Iy signals were processed with a 5 point moving-window-average.

4. Discussion

Method #1

We demonstrated that our ratiometric approach laid out as method #1 enabled us, for the first time to our knowledge, to monitor the relative change of the χ tensor components separately during a change of molecular state. We showed that both components underwent an unequal increase from relaxed to rigor state (Fig. 2(A)). This fact reveals that the increase of the parameter γ towards a contracted state [6, 25] is based on the unequal increase of both components and not, e.g., on a decrease of the χ(xyy) component. The increase of χ(xyy) also causes an absolute increase of the SHG signal as observed in this work and as described by Nucciotti and associates [25].

To compare our values to data from prior studies we calculated the ratio of the γ values corresponding to relaxed and rigor state with Eq. (5). The resulting value of 1.53 was in good agreement with Schürmann *et al*. [6], γ(relax) 0.501, γ(rigor) 0.733, ratio of γ 1.46; and Nucciotti *et al.* [25], γ(relax) 0.46, γ(rigor) 0.68, ratio of γ 1.48. However, the control values shown in Fig. 2(B) (mean values: γ(relax) 0.61, γ(rigor) 0.92) calculated with Eq. (8) were 22-35% higher than the γ values referenced above. One potential reason might have been a movement of the samples during change of solution and change of state (see section 2.3). Therefore, the fiber bundles might not have stayed put in the object plane, leading to an additional axial z-dependency. This behavior could also explain the higher rigor values of the first four fibers as they were measured in the same sample. In Fig. 6 a theoretical estimation of the influence of an axial misalignment of the sample is shown. To quantify this influence, we assume an oblique incident beam instead of an axial misalignment of the sample. Thus, the electrical field has an additional z-component Ez in the coordinate system of the sample. Another assumption is that the entire signal is still collected by the detector. The SHG signal intensities at polarization angles of 0° and 90° are now given by:

$$\begin{aligned} I^*(0°,\Delta\xi) &= B\chi_{xyy}^2[(\gamma\cos^2(\Delta\xi)+\sin^2(\Delta\xi))^2+\sin^2(2\Delta\xi)], \\ I^*(90°,\Delta\xi) &= B\chi_{xyy}^2. \end{aligned} \tag{9}$$

$\Delta\xi$ is the angle of the axial deviation and I* denotes again the actual measured intensities. Note that the (I(90°))* term remains unaffected. Using these new expressions of Eq. (9) to calculate γ with Eq. (8) of the control leads to false values of γ as shown in Fig. 6. Hence, with this simplified model we can derive an estimation of the influence of axial misalignments of the sample. We can observe that such axial angular errors can have a major impact on the results for higher axial deviations resulting in increased γ values. Note that Schurmann *et al.* showed that neglecting an axial component of the incident laser beam due to a high NA results in increased γ values [6].

#254217 Received 18 Nov 2015; revised 18 Dec 2015; accepted 18 Dec 2015; published 15 Jan 2016

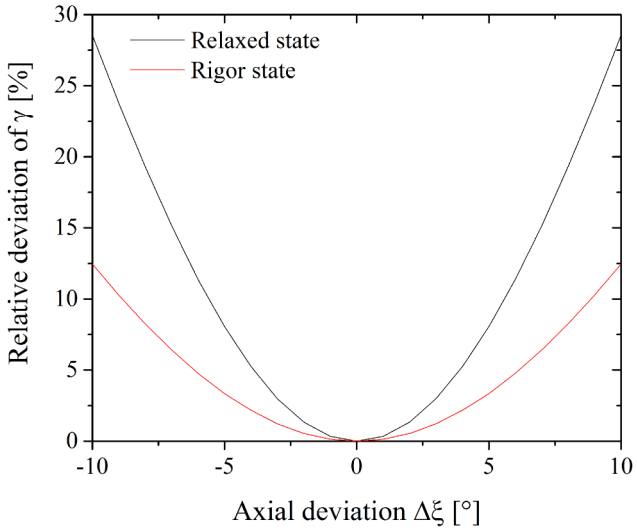

Fig. 6. Theoretical estimation of the impact of an axial misalignment of the sample on the γ value with a simplified model assuming an oblique incident laser beam.

By calculating the mean signal values for the 0° and 90° measurements of the method #2 control (Fig. 3(B)) we could estimate values for samples that were lying completely in the object plane (no axial z-dependency): for the χ(xxx) and the χ(xyy) component we got 2.2 and 1.3, respectively. This result could suggest that the relative change of the tensor components is not as sensitive to axial dependencies as the absolute values are.

Our approach has the potential to give new insights into the structural dynamics of proteins during a change of state, e.g., the contraction of muscle. For example, Leray *et al.* [35] proposed a correlation of the tensor components to the molecular hyperpolarizability tensor β:

$$\begin{aligned} \chi_{xxx} &= N_S \beta_e \cos^3\theta_e, \\ \chi_{xyy} &= \frac{1}{2} N_S \beta_e \cos\theta_e \sin^2\theta_e. \end{aligned} \tag{10}$$

Here, N_s is the density of active harmonophores, β_e is the effective dominant axial coefficient of the molecular tensor and θ_e is the effective angle of harmonophore orientation. Tiaho *et al.* [30] used this approach to investigate the organization of harmonophores in myosin- and collagen-rich tissue by determinating θ_e which they correlated to the helical pitch angle and which is connected to the parameter γ by [28, 30]:

$$\gamma = \frac{2}{\tan^2\theta_e}. \tag{11}$$

Combining the approach laid out in Eq. (10) with our approach of method #1 we get information about the molecular axial coefficient during a change of state:

$$\begin{aligned} \frac{\beta_e^{(S2)}}{\beta_e^{(S1)}} &= \frac{\chi_{xxx}^{(S2)}}{\chi_{xxx}^{(S1)}} \frac{\cos^3\theta_e^{(S1)}}{\cos^3\theta_e^{(S2)}}, \\ \frac{\beta_e^{(S2)}}{\beta_e^{(S1)}} &= \frac{\chi_{xyy}^{(S2)}}{\chi_{xyy}^{(S1)}} \frac{\cos\theta_e^{(S1)} \sin^2\theta_e^{(S1)}}{\cos\theta_e^{(S2)} \sin^2\theta_e^{(S2)}}. \end{aligned} \tag{12}$$

#254217 Received 18 Nov 2015; revised 18 Dec 2015; accepted 18 Dec 2015; published 15 Jan 2016

Note that we should get the same result for both tensor ratios. Inserting the values for the effective orientation of the harmonophores calculated with Eq. (11) using the γ values of the control of method #1 (Fig. 2(B)) or the values measured with method #2 (Fig. 3(A)) we calculated the relative change of β_e during a change from relaxed to rigor state with Eq. (12). The results were 1.47 for the χ(xxx) component (1.38 for method #2 values) and 1.45 (1.39) for the χ(xyy) component, respectively. The calculations rendered comparable values for both tensor components and substantiated our results.

This demonstrates that our approach of method #1 has the potential to deliver new information of structural molecular dynamics. For instance, Rouède *et al.* [36] report that their data support the assumption of a second emitter in collagen. This leads to a more complex interpretation of the structural dynamics, calling for new approaches.

Although method #1 may also be applicable to high speed measurements we found it was not very suitable for this purpose in practice. The method should be relatively insensitive to sideways movements because the signals are collected in the local minima of the SHG polarization dependency. However, any movement like the change of focal plane will lead to artifacts that cannot be distinguished from signals due to change of state. Hence, we chose the polarimetric approach with intrinsic normalization of method #2 for high speed monitoring of the contraction process.

Method #2

We demonstrated that we were able to measure values for γ at different contraction states with our polarimetric approach of method #2. The results for rigor and relaxed state of non-dynamic measurements (Fig. 3(A)) were in good agreement to the control (Fig. 3(B)) and to the values obtained in prior studies [6, 25] (see above). Note that Nucciotti *et al.* [25] demonstrated that the values for the relaxed state are independent of the sarcomere length and that the rigor values decrease at lengths over 2.4 µm. Schürmann *et al.* [6] did not find a correlation until approximately 2.6 µm. We also compared the difference $\Delta\gamma = \gamma^{(rigor)} - \gamma^{(relaxed)}$, as the relative change is of higher interest for biological applications and as systematic errors of the setup should have less impact. We found a difference of 0.25 for method #1 values and 0.3 for the control compared to 0.232 [6] and 0.22 [25].

Measuring at different angles of polarization (Table 1) we demonstrated that our chosen angle of polarization of $\alpha = 18°$ is in the region of minimized sensitivity to movement of the sample. It was therefore a suitable choice for our experiments. The results at 18° for the exact and inclined ROIs matched best with the control values and the standard deviations were minimal. As expected the control was less susceptible to angular errors of the sample as the signals were collected in the local minima of the SHG polarization dependency.

We analyzed the impact of misalignment of the sample at an angle of polarization of 18° (Fig. 4). This test of accuracy was important as sideways movement of the sample can lead to false values for changes of γ because the angle between the sample and the polarization and the PBS is changed. In Fig. 4(A) the change of γ due to angular errors and the modeled values calculated with Eq. (7) are shown. In contrast to the modeled values it should be noted that the experimental data included an inaccuracy of choosing the ROI. A large inaccuracy of choosing the ROI can lead to opposite signs of $\Delta\alpha$ and $\Delta\beta$ if they have differing size and thus can compromise the optimum measuring angle. In this regard, an intentionally detuning might be considered as for dynamic measurements the relative change is of higher interest than the absolute values are.

With respect to the impact of angular errors of the sample we observed an asymmetry (Fig. 4(B)). Angular errors in the positive direction can severely disturb the measurements if major movements occur. At this point, analyzing the Ix and Iy polarization signals is very useful to distinguish a false change of γ from a real event. Experimental data are shown in Fig. 4(C), the modeled values in panel D. A 'real' increase of γ induced by a change of state of myosin towards a contracted state is correlated to an increase of both polarization signals as both tensor components increase (see method #1 Fig. 2(A)). In addition, the increase of the

#254217 Received 18 Nov 2015; revised 18 Dec 2015; accepted 18 Dec 2015; published 15 Jan 2016

Ix component is larger and yields an increase of the value of γ (see Eq. (2) and Eq. (6)). In panel C and D of Fig. 4 we can observe that both signals are decreasing for positive angular errors. The decrease of Iy is larger. This explains the strong increase of γ here. Angular errors of the sample in the negative direction have no major impact for smaller movements of the sample. Both signals undergo a comparable increase, leading to only minor changes of γ. Also, the deviation of γ is partially negative; this event can be directly identified as a false signal. Thus, analyzing the Ix and Iy signals is a powerful tool to distinguish false from real γ changes. Yet, a good cell immobilization is mandatory for high speed line scan measurements, such that only minor movements can occur, that the same region can be monitored during the experiment or that movements out of focus are prevented.

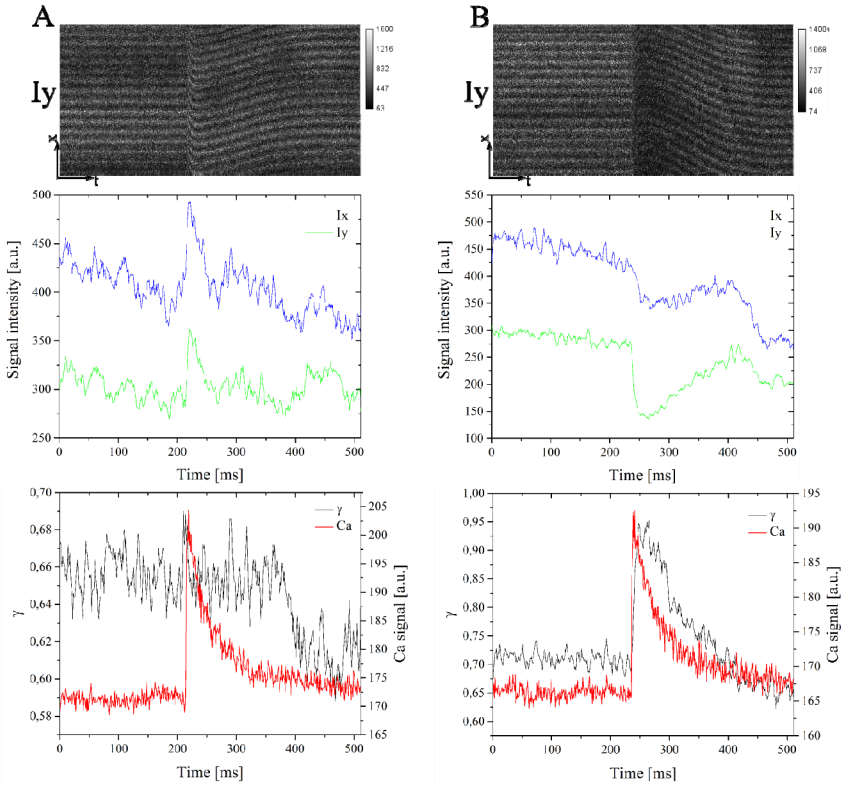

Fig. 7. Examples of moving artifacts during contraction measured on an electrically stimulated IO fiber that was not embedded in agarose. γ signal, polarization components signals, calcium signal and Iy line scan images (29.76 µm x 512 ms) are displayed. (**A**) Movement to the negative direction. (**B**) Movement to the positive direction. γ, Ix and Iy were processed with a 5 point moving-window-average. For visualization purposes pixels with large gray values are displayed in white in the images (occurrence <0.1% of total number of pixels).

Two examples of movements during a measurement are shown in Fig. 7. The IO fiber was not embedded in agarose and could move freely. Calcium and γ signals are depicted in red and black, respectively, with the corresponding Iy line scan image and the Ix and Iy signal marked in blue and green, respectively. The γ, Ix and Iy signals were processed with a 5 point moving-window-average. In both line scan images we observed strong movement. Figure 7(A) corresponds to the situation of a movement in the negative direction: both signals underwent a comparable increase thus no change of the γ signal was distinguishable as movement in the negative direction only has a minor impact. Figure 7(B) corresponds to a movement in the positive direction: we observed a strong increase of γ correlating with the calcium signal. At first sight, this increase could easily be interpreted as real signal. However,

#254217 Received 18 Nov 2015; revised 18 Dec 2015; accepted 18 Dec 2015; published 15 Jan 2016

both signals were decreasing and the decrease of Iy was larger, so that this event was identified as a false change of γ.

Both measurements showed signal changes after the calcium peak that could not be distinguished. Both changes led to a decrease of γ because of a higher increase of Iy in panel A and because of a stronger decrease of Ix in panel B. A probable explanation is the repositioning of the cell after the twitch as they were not immobilized. This would lead to a misalignment of the sample and/or an axial dependency. The high resting γ values at the beginning suggest an existing axial dependency (cells not lying in the focal plane). Repositioning of the cells after the twitch could have changed this dependency leading to the lower resting γ base lines.

We demonstrated the application of method #2 for high speed 1D line scans and monitored the molecular dynamics of a contraction process with millisecond time resolution using fSHG microscopy in Fig. 5. Different points support that we have indeed measured the molecular dynamics of myosin by monitoring the change of the parameter γ: First, we observed no major movements in the line scan images (cf. Fig. 7) indicating that if only minor sideways movement occurred. Second, the Ix and Iy signals behaved as predicted, the increase of Ix was substantially larger than the one of Iy: for instance, in panel D we can see that the increase of Iy was not distinguishable from the background oscillation. If there was a sideways movement of the cell it would be in the negative direction as the signals were increasing and not decreasing as they would for the positive direction. In the negative direction however, only minor false changes of γ occur for minor movements of the sample as were observed in the line scan images. In this measurement we detected relative changes of γ of approximately 8% to 16%. Next, we observed an increase of γ when electrical stimulation was increased from 16 V to 28V. Furthermore, the change of γ behaved as we expected while force is produced [26]: The change of γ was correlated with the calcium peak, reaching its maximum approximately on average 27 ms behind the calcium peak. Finally, the process was taking approximately 123 ms on average, which is in the range of the normal contraction process. Thus, we conclude that the molecular dynamics of a contraction process has been observed.

Monitoring of the molecular dynamics has high potential for new insights of the contraction process under physiological or pathological conditions. It also can supplement existing methods like single fiber force measurements as a change of the parameter γ can be correlated to the produced force and occupancy of different myosin states [25]. In addition, slower 2D scan measurements can be used to monitor e.g. cooperation or proliferation during contraction as was demonstrated by Psilodimitrakopoulos *et al.* [28].

The advantages of our methods presented in this study are the use of linear polarized incident light and the use of a detection system with one or two PMTs only. Linear polarization can be produced in high quality and, additionally, residual ellipticity can be compensated for [37]. A connected influence to consider is birefringence of the tissue that can lead to a phase shift of the incident light and/or the SHG signal [32, 33]. We may consider the latter in our setup and introduce a phase shift in Eq. (7) by multiplicating $\cos(\delta)$ to the mixed terms $\sqrt{I_x I_y}$. In this situation, the mixed term vanishes only in the case of perfect circular polarization. In this model, however, this additional component had no major impact on our results.

A detection system with two PMTs only can be easily integrated in a standard laser scanning microscope. Splitting the signal to fewer detectors is advantageous with respect to the signal-to-noise ratio. Yet, a drawback of our method is the angle dependency of the signal that can lead to motion artifacts. But as mentioned above, a careful choice of the angle of polarization and the monitoring of the individual polarization signals can minimize this impact to a sufficiently low level.

As mentioned in the 'Theoretical considerations' above, common approximations were made for this first proof of principle of monitoring relative changes in the SHG signal during contraction. However, within this context, resulting values for γ cannot be read absolutely

#254217 Received 18 Nov 2015; revised 18 Dec 2015; accepted 18 Dec 2015; published 15 Jan 2016

and must be interpreted with caution: A high NA [6] or a tilt of the S1-S2 myosin segment [25] will result in an additional axial field [6, 31] or tensor component [38], respectively. Model functions observing these effects but using the same raw data will lead to significantly different values of γ.

For future research we aim for an optimization of our setup with respect to working distance, cell manipulation and automated cell alignment to enable larger series of experiments and a more effective assessment of the dynamic molecular behavior of muscle contraction.

5. Conclusion

In conclusion, using polarization-resolved SHG microscopy, we present two new experimental methods to assess structural and temporal dynamic information on the molecular level of the contraction process under *ex vivo* conditions. In contrast to prior approaches, incident linear polarization is used. Additionally, data from one angle of polarization only and one or two detectors are needed. We demonstrate significant improvement with respect to temporal resolution and ease of use. Our methods have therefore the potential to bridge the missing link between *in vitro* single molecule experiments and *ex vivo* macroscopic force output measurements or *in vivo* applications.

Acknowledgments

M.F. acknowledges the support by a PhD scholarship of the Evangelisches Studienwerk Villigst e.V., member of the talent program network of the German Federal Ministry of Education and Research. We thank Cornelia Weber for sharing her knowledge of cells and solutions.